ChemComm

COMMUNICATION

View Article Online
View Journal | View Issue

Cite this: *Chem. Commun.*, 2015, **51**, 1631

Received 20th October 2014,
Accepted 2nd December 2014

DOI: 10.1039/c4cc08266d

www.rsc.org/chemcomm

Enhanced performance of dye-sensitized solar cells based on TiO_2 nanotube membranes using an optimized annealing profile†

F. Mohammadpour,[a] M. Moradi,[a] K. Lee,[b] G. Cha,[b] S. So,[b] A. Kahnt,[c] D. M. Guldi,[c] M. Altomare[b] and P. Schmuki*[bd]

We use free-standing TiO_2 nanotube membranes that are transferred onto FTO slides in front-side illuminated dye-sensitized solar cells (DSSCs). We investigate the key parameters for solar cell arrangement of self-ordered anodic TiO_2 nanotube layers on the FTO substrate, namely the influence of the annealing procedure on the DSSC light conversion efficiency. The results show that using an optimal temperature annealing profile can significantly enhance the DSSC efficiency (in our case η = 9.8%), as it leads to a markedly lower density of trapping states in the tube oxide, and thus to strongly improved electron transport properties.

TiO_2-based dye-sensitized solar cells (DSSCs) have attracted much attention in the last few decades mainly because of their low cost of fabrication and relatively high efficiency compared to devices based on other inorganic semiconductors. Cell efficiencies up to 12.3% were reached with Grätzel-type solar cells by using dye-sensitized TiO_2 nanoparticle (NP) films as photo-anodes.[1,2] Except for an optimal light harvesting by the dye and injection of carriers into the TiO_2 scaffold, a key element for the cell efficiency is the transport of electrons through the photo-anode (*vs.* various recombination pathways). In this context, the charge carrier mobility and cell efficiency are inherently limited in a TiO_2 nanoparticle (NP) film by the "random walk" electron transport through the network.[3–5]

Therefore, one-dimensional (1D) architectures such as high-aspect ratio nanowire,[6,7] nanorod,[8,9] and nanotube[3,10–15] arrays have been investigated as photo-anodes for DSSCs, in expectation of a directional and thus faster electron transport. Anodic TiO_2 nanotube (NT) layers have attracted wide attention primarily due to their geometry but also due to their long term stability and facile fabrication. The process of growing tube arrays is based on a simple anodization of a piece of Ti metal under self-organizing electrochemical conditions.[16]

In principle, the resulting aligned nanotubular oxide layers can directly be used in Grätzel type DSSCs adopting a so called "back-side" illumination configuration, where the Ti metal represents the back contact to the dye-sensitized NT layer (see Scheme S1(a) in the ESI†).

Nevertheless, one would expect a front-side illumination configuration of the TiO_2 nanostructures (Scheme S1(b) and (c), ESI†) to reach higher cell efficiencies compared to a back-side configuration, this is because the photo-anode in this case can be irradiated through the FTO glass so that light losses due to light absorption in the electrolyte and in the Pt coating of the counter electrode are minimized.

In order to establish a front-side illumination configuration with anodic TiO_2 NT layers, either Ti metal is sputtered on optically transparent conductive substrate glass (FTO) and completely anodized until a transparent NT layer is formed,[17] or NT layers are detached from the Ti substrate as free-standing membranes and are transferred onto FTO slides. To date the latter approach, that is, the layer transfer, led to higher cell performance compared to sputtering Ti layers on FTO.[18–20]

A range of different strategies were developed for transferring and arranging tube membranes for their use in DSSCs. Not only tube length and various decoration techniques but also different geometries and configurations, such as open/closed tube bottom and tube bottom up/down (illustrated in Scheme S1 in the ESI†), were explored.[18,20–24] In all these studies, as grown nanotubes are typically converted to anatase by suitable annealing. In spite of this, a thorough study of the annealing conditions of the tubes (including temperature ramping rates) is still missing. This is surprising as earlier reports have shown that the annealing rate can, for instance, drastically affect the tube wall morphology, the chemical properties[25] and the density of grain internal trapping states,[26,27] and thus could be expected to significantly affect the electron transport properties.

Therefore, the present work explores the feasibility to achieve higher efficiencies for front-side illuminated DSSCs, particularly

[a] *Physics Department, College of Science, Shiraz University, Eram Street, 71454 Shiraz, Iran*
[b] *Department of Material Science and Engineering, WW4-LKO, University of Erlangen-Nuremberg, Martensstrasse 7, D-91058 Erlangen, Germany. E-mail: schmuki@ww.uni-erlangen.de; Fax: +966-49-9131-852-7582; Tel: +966-49-9131-852-7575*
[c] *University of Erlangen-Nuremberg, Egerlandstrasse 3, D-91058 Erlangen, Germany*
[d] *Department of Chemistry, King Abdulaziz University, Jeddah, Saudi Arabia*

† Electronic supplementary information (ESI) available. See DOI: 10.1039/c4cc08266d

by improving the electron transport properties of the tubes under optimized annealing conditions (specifically addressing also temperature ramping).

In order to evaluate various solar cell configurations, we produced free-standing membranes with a number of transfer techniques, and we optimized the annealing treatment of the nanotube layers. Under optimized thermal treatment that implies, namely, a controlled heating rate, TiO_2 NT membranes in an optimal configuration exhibit improved intrinsic electronic properties and thus lead to photo-anodes for front-side illuminated DSSCs with a significant increase in their efficiency.

TiO_2 nanotube layers were formed by anodization of Ti foils at 60 V for 1 h in an ethylene glycol-based electrolyte (containing 0.15 M of NH_4F and 3 vol% of DI water). A re-anodization approach (see the ESI† for additional details) was used to detach the nanotube layers from the Ti substrate. This allows nanotube membranes to be successfully lifted off and transferred as intact layers onto TiO_2 NP-coated FTO glass.

Screening experiments were carried out by fabricating photo-anodes with 20 μm-thick free-standing tube membranes that were transferred on FTO slides in two different geometries, that are, tube-top-up and tube-top-down configurations, as illustrated in Scheme S1(b) and (c), ESI.† These photo-anodes were crystallized (see XRD data in Fig. S1, ESI†) and then were used for fabricating DSSCs. The preliminary experiments (see results in Fig. S2, ESI†) show that the tube-top-down configuration (Fig. 1(a)) of the photo-anode along with an annealing temperature of 500 °C represents the experimental conditions leading to cells with higher efficiencies (data are discussed in the ESI†).

Therefore, these conditions were adopted for all further experiments. Specifically, the crystallization of the tube membranes at different heating/cooling rates (10, 30 and 60 °C min^{-1}) was investigated in detail. In every case, the XRD patterns of different photo-anodes (Fig. S1(a), ESI†) show the TiO_2 nanotube membranes to consist of pure anatase phase regardless of the heating/cooling rate.

From these layers, the DSSCs were fabricated as reported in the experimental section (see the ESI†). A ''reference cell'' was also fabricated by using a 20 μm-thick TiO_2 NP layer as a photo-anode instead of the detached nanotube membranes.

Fig. 1(b) shows the *J–V* curves of the cells and summarizes their photovoltaic characteristics measured under simulated AM 1.5 (100 mW cm^{-2}) front-side illumination. Clearly, the cell efficiency is strongly affected by the annealing conditions (ramp rate), that is, a significant enhancement of the photovoltaic performance is observed when increasing the heating rate from 10 to 30 °C min^{-1}. In particular, a heating rate of 30 °C min^{-1} leads to a significant improvement of the solar light conversion efficiency up to 9.79%. All efficiency values reported here were obtained by measuring the cell efficiency under defined active area conditions (see detailed discussion in the ESI†) and are in line with IPCE measurements (see Fig. S3 in the ESI†).

A further increase of the heating rate up to 60 °C min^{-1} leads to a decrease of the cell performance, although the cell efficiency is still markedly higher than measured under slow ramping conditions (*e.g.*, 10 °C min^{-1}). The results in Fig. 1(b) furthermore show that an optimized annealing of the tube membranes (*e.g.*, heating rate of 30 °C min^{-1}) led to cells that were more efficient than a DSSC assembled from a TiO_2 NP film (this photo-anode was annealed under the same conditions as adopted for crystallizing the membranes).

A factor that commonly strongly affects the photovoltaic performance is the specific dye-loading, that is, the larger the amount of dye loaded by chemisorption on the TiO_2 surface, the higher is the light harvesting efficiency and thus the cell efficiency. However, data in Fig. 1(b) clearly show that the highest dye-loading was measured for the TiO_2 NP-based photo-anode (this is in line with commonly observed lower BET areas for tube layers compared to nanoparticles). In other words, the dye-loading cannot be the key to explain the significantly higher efficiency of cells fabricated with rapidly-annealed tubes.

Therefore, IMPS measurements were performed in order to assess the electron transport properties of the different dye-sensitized photo-anodes (Fig. 1(c)). Data in Fig. 1(c) show that a significant improvement of the electron transport was obtained for DSSCs that were fabricated with membranes crystallized by rapid annealing (*i.e.*, 30 and 60 °C min^{-1}). Similar results were obtained also when performing IMPS measurements on the bare photo-anodes (*i.e.*, without dye-sensitization), confirming that rapid annealing of the tubes enables improved charge transport properties (see Fig. S4 in the ESI†). Yet, it is worth noting that (i) the tubes annealed at 30 °C min^{-1} showed markedly faster electron transport properties compared to those treated by an even faster ramping (*i.e.*, 60 °C min^{-1}), and (ii) the 20 μm-thick TiO_2 NP layer used for fabricating the reference cell always showed worse charge transport properties (*i.e.*, slower electron transport and faster charge recombination) compared to the NT-based cells, regardless of the annealing conditions.

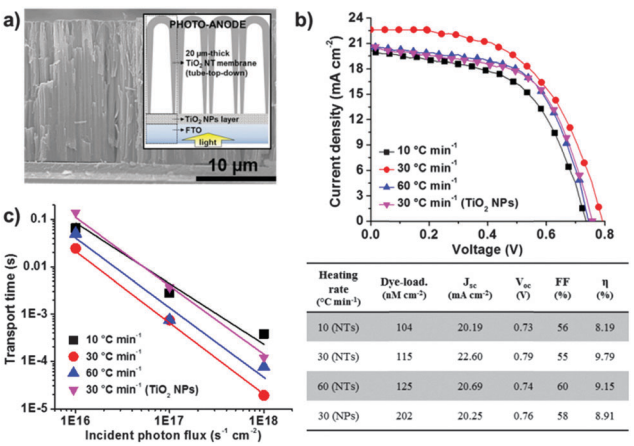

Heating rate (°C min^{-1})	Dye-load. (nM cm^{-2})	J_{sc} (mA cm^{-2})	V_{oc} (V)	FF (%)	η (%)
10 (NTs)	104	20.19	0.73	56	8.19
30 (NTs)	115	22.60	0.79	55	9.79
60 (NTs)	125	20.69	0.74	60	9.15
30 (NPs)	202	20.25	0.76	58	8.91

Fig. 1 (a) Cross-sectional SEM image of a photo-anode consisting of a 20 μm-thick TiO_2 NT membrane that was fabricated by the re-anodization approach and transferred in tube-top-down configuration on a FTO slide coated with a 2 μm-thick TiO_2 NP film. Inset: a sketch of the photo-anode configuration adopted for assembling the DSSCs; (b) *J–V* curves and a summary of the photovoltaic characteristics of the different DSSCs measured under simulated AM 1.5 front-side illumination; (c) IMPS measurements performed on the different DSSCs (the continuous lines are a guide to the eye).

The latter result, in particular, shows that the geometric features of the TiO_2 photo-anode largely affect the charge carrier mobility which in turn influences the cell efficiency. In other words, the electron transport across a TiO_2 photo-anode can largely benefit from the use of one-dimensional TiO_2 NT arrays in comparison to slower characteristics observed for NP layers.[3–5,10–12] By taking into consideration that the cell efficiency may strongly relate to the structure of the TiO_2 scaffold, a morphological evaluation of the crystalline photo-anodes annealed with different ramping rates was carried out by performing scanning and transmission electron microscopy (SEM and TEM) (see Fig. 2 and additional description in the ESI†).

These investigations show that a clear separation of the inner and outer shells of the nanotubes and a corrugated structure of the walls (with clearly visible grain boundaries) are obtained when the tube membranes are annealed with a heating rate of 10 °C min^{-1} (see Fig. 2(a) and (b)). The separation of inner and outer shells could not be observed for rapid annealing and the annealing process merged the two shells instead, so that an apparently "single-walled" tubular structure was formed upon crystallization, as shown in Fig. 2(c)–(f). These results are well in line with previous reports.[25,28,29]

In order to elaborate the large difference in cell efficiencies and electron transport properties further we additionally investigated the differently annealed tubes by transient absorption spectroscopy based on femtosecond (fs) pump–probe experiments (see the ESI† for experimental details).

The results are compiled in Fig. 3(a)–(d) (and Fig. S7(a) and (b), ESI†). In general, the spectra can be separated into three components (holes, trapped and free electrons – see ESI†), this being well in line with the literature on TiO_2.[27,30–33] The fitting results, which provide the corresponding lifetime for holes, trapped- and free-electrons, are reported in the table in Fig. 3(e) (and Fig. S7(c), ESI†). Overall, clear differences in the lifetime values can be observed for the free-electrons (*i.e.*, τ_3). Precisely, the lifetime of free-electrons is markedly increased when the tube scaffolds were annealed with ramping of 30 °C min^{-1} compared to 10 °C min^{-1}. These results are well in line with relative solar cell efficiencies and IMPS data that show faster electron transport for rapidly annealed tubes.

A slight increase of free-electron lifetime was also observed by a further increase of the annealing rate up to 60 °C min^{-1} (Fig. S7(c), ESI†). However, for solar cells fabricated from these tubes, a slight drop of efficiency was observed compared to tubes annealed at 30 °C min^{-1}, which is in agreement with the considerably (*in situ*) slower electron transport (IMPS results) of the former.

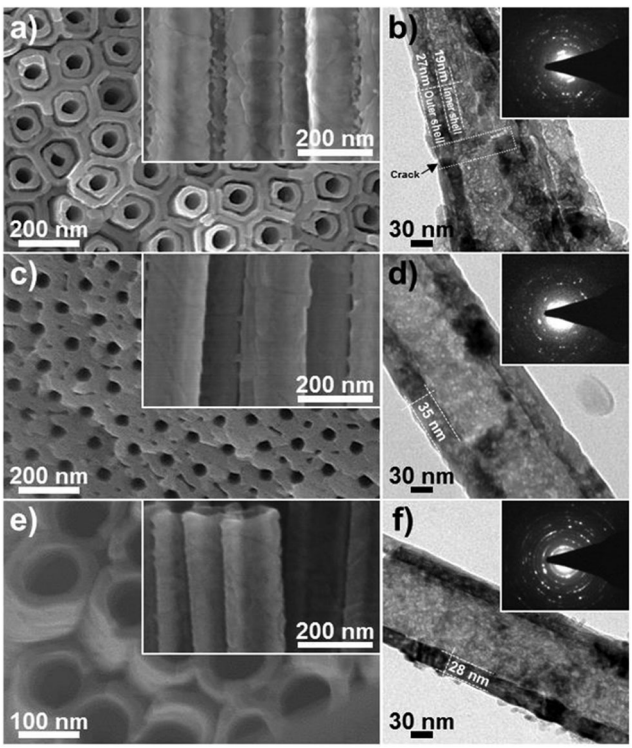

Fig. 2 High-magnification top view SEM images of TiO_2 nanotube membranes annealed in air at 500 °C by using heating rates of (a) 10, (c) 30 and (e) 60 °C min^{-1}. The images were taken at middle height along the length of the tubes after cracking the anodic layers. Insets: relative high-magnification cross-sectional SEM images of the nanotubes; TEM images of tubes annealed in air at 500 °C by using heating rates of (b) 10, (d) 30 and (f) 60 °C min^{-1}. Insets: relative SAED patterns showing the typical reflections of the TiO_2 anatase phase.

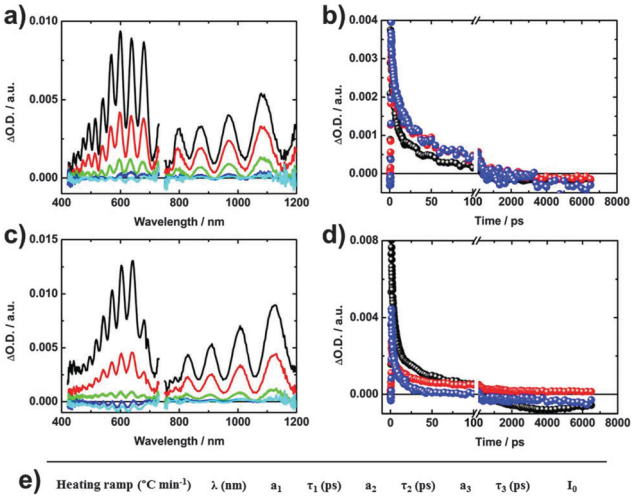

e)

Heating ramp (°C min^{-1})	λ (nm)	a_1	τ_1 (ps)	a_2	τ_2 (ps)	a_3	τ_3 (ps)	I_0
10	550	0.18	4.4	0.33	35.6	0.49	521	- 1.55 E^{-4}
	800	0.37		0.46		0.17		- 7.00 E^{-5}
	1200	0.37		0.45		0.18		- 1.69 E^{-4}
30	550	0.51	4.3	0.27	36.7	0.22	1110	- 8.04 E^{-4}
	800	0.43		0.45		0.12		1.36 E^{-4}
	1200	0.61		0.33		0.06		- 3.35 E^{-4}

Fig. 3 (a) and (c) Differential absorption spectra (visible and near-infrared) measured by femtosecond flash photolysis (258 nm) at different time delays of 1 ps (black), 10 ps (red), 100 ps (green), 1000 ps (blue), and 6500 ps (cyan); (b) and (d) relative absorption time profiles of the spectra (a) and (c) at 550 nm (black), 800 nm (red) and 1200 nm (blue) corresponding to absorption of holes, trapped-electrons and free electron, respectively. Data in (a)–(d) were measured for *ca.* 3 μm-thick TiO_2 nanotube layers (grown on quartz slides) that were annealed at 500 °C with heating rates of (a), (b) 10 °C min^{-1} and (a), (b) 30 °C min^{-1}; (e) data obtained by fitting the decay transient curves to three exponential functions (at 550, 800 and 1250 nm) in order to distinguish the contributions of the different transient species (*i.e.*, holes, trapped-electrons and free electron).

Overall, the results of fs pump–probe spectroscopy and IMPS measurements show that a rapid annealing of anodic TiO_2 nanotubes enables superior electronic properties that can be ascribed to a lower density of trapping states.[26,27] Such enhanced electron transport of rapidly-annealed tubes may be related to the robust, crack-free and "single-walled" morphology. In contrast, slow annealing led to tubes characterized by a relatively large number of cracks and this feature may induce charge recombination and limit the electron lifetime, which in turn detrimentally affect the one-dimensional electron transport.

Free-standing TiO_2 nanotube membranes were fabricated to be used as photo-anodes in front-side illuminated DSSCs. We showed that several experimental factors strongly affect the solar cell efficiency. In particular, the heating rate used during the crystallization of the photo-anodes largely influenced the structural features of the tubes and their charge carrier transport properties which in turn affect, to a large extent, the solar light conversion efficiency of the device.

The authors would like to acknowledge ERC, DFG and the Erlangen DFG cluster of excellence for financial support. Helga Hildebrand is gratefully acknowledged for valuable technical help. Also the financial support from the Iran Ministry of Science, Research and Technology is gratefully acknowledged.

Notes and references

1 B. O'Regan and M. Grätzel, *Nature*, 1991, **353**, 737.
2 A. Yella, H.-W. Lee, H. N. Tsao, C. Yi, A. K. Chandiran, Md. K. Nazeeruddin, E. W.-G. Diau, C.-Y. Yeh, S. M. Zakeeruddin and M. Grätzel, *Science*, 2011, **334**, 629.
3 P. Roy, D. Kim, K. Lee, E. Spiecker and P. Schmuki, *Nanoscale*, 2010, **2**, 45.
4 E. J. W. Crossland, N. Noel, V. Sivaram, T. Leijtens, J. A. Alexander-Webber and H. J. Snaith, *Nature*, 2013, **495**, 215.
5 S. So and P. Schmuki, *Angew. Chem., Int. Ed.*, 2013, **52**, 7933.
6 Q. Shen, T. Sato, M. Hashimoto, C. Chen and T. Toyoda, *Thin Solid Films*, 2006, **499**, 299.
7 M. Adachi, Y. Murata, J. Takao, J. Jiu, M. Sakamoto and F. Wang, *J. Am. Chem. Soc.*, 2004, **126**, 14943.
8 S. H. Kang, S.-H. Choi, M.-S. Kang, J.-Y. Kim, H.-S. Kim, T. Hyeon and Y.-E. Sung, *Adv. Mater.*, 2008, **20**, 54.
9 S. Pavasupree, S. Ngamsinlapasathian, Y. Suzuki and S. Yushikawa, *J. Nanosci. Nanotechnol.*, 2006, **6**, 3685.
10 J. M. Macák, H. Tsuchiya, A. Ghicov and P. Schmuki, *Electrochem. Commun.*, 2005, **7**, 1133.
11 A. Ghicov, S. P. Albu, R. Hahn, D. Kim, T. Stergiopoulos, J. Kunze, C.-A. Schiller, P. Falaras and P. Schmuki, *Chem. – Asian J.*, 2009, **4**, 520.
12 S. So, K. Lee and P. Schmuki, *J. Am. Chem. Soc.*, 2012, **134**, 11316.
13 K. Zhu, N. R. Neale, A. Miedaner and A. J. Frank, *Nano Lett.*, 2007, **7**, 69.
14 J. R. Jennings, A. Ghicov, L. M. Peter, P. Schmuki and A. B. Walker, *J. Am. Chem. Soc.*, 2008, **130**, 13364.
15 R. P. Lynch, A. Ghicov and P. Schmuki, *J. Electrochem. Soc.*, 2010, **157**, G76.
16 P. Roy, S. Berger and P. Schmuki, *Angew. Chem., Int. Ed.*, 2011, **50**, 2904.
17 G. K. Mor, K. Shankar, M. Paulose, O. K. Varghese and C. A. Grimes, *Nano Lett.*, 2006, **6**, 215.
18 Q. Chen and D. Xu, *J. Phys. Chem. C*, 2009, **113**, 6310.
19 B.-X. Lei, J.-Y. Liao, R. Zhang, J. Wang, C.-Y. Su and D.-B. Kuang, *J. Phys. Chem. C*, 2010, **114**, 15228.
20 M. Dubey, M. Shrestha, Y. Zhong, D. Galipeau and H. He, *Nanotechnology*, 2011, **22**, 285201.
21 K.-H. Chung, Md. Mahbubur Rahman, H.-S. Son and J.-J. Lee, *Int. J. Photoenergy*, 2012, **2012**, 1.
22 J. Lin, J. Chen and X. Chen, *Nanoscale Res. Lett.*, 2011, **6**, 475.
23 L.-L. Li, Y.-J. Chen, H.-P. Wu, N. S. Wang and E. W.-G. Diau, *Energy Environ. Sci.*, 2011, **4**, 3420.
24 C.-J. Lin, W.-Y. Yuab and S.-H. Chien, *J. Mater. Chem.*, 2010, **20**, 1073.
25 S. P. Albu, A. Ghicov, S. Aldabergenova, P. Drechsel, D. LeClere, G. E. Thompson, J. M. Macák and P. Schmuki, *Adv. Mater.*, 2008, **20**, 4135.
26 C. Richter and C. A. Schmuttenmaer, *Nat. Nanotechnol.*, 2010, **5**, 769.
27 A. Kahnt, C. Oelsner, F. Werner, D. M. Guldi, S. P. Albu, R. Kirchgeorg, K. Lee and P. Schmuki, *Appl. Phys. Lett.*, 2013, **102**, 233109.
28 H. Mirabolghasemi, N. Liu, K. Lee and P. Schmuki, *Chem. Commun.*, 2013, **49**, 2067.
29 N. Liu, H. Mirabolghasemi, K. Lee, S. P. Albu, A. Tighineanu, M. Altomare and P. Schmuki, *Faraday Discuss.*, 2013, **164**, 107.
30 A. Hagfeldt and M. Grätzel, *Chem. Rev.*, 1995, **95**, 49.
31 X. Yang and N. Tamai, *Phys. Chem. Chem. Phys.*, 2001, **3**, 3393.
32 T. Yoshihara, R. Katoh, A. Furube, Y. Tamaki, M. Murai, K. Hara, S. Murata, H. Arakawa and M. Tachiya, *J. Phys. Chem. B*, 2004, **108**, 3817.
33 Y. Tamaki, A. Furube, M. Murai, K. Hara, R. Katoh and M. Tachiya, *Phys. Chem. Chem. Phys.*, 2007, **9**, 1453.

